

Planning and Model-Based Control for Mobile Manipulators

Evangelos Papadopoulos and John Poulakakis

Department of Mechanical Engineering
National Technical University of Athens, 15780 Zografou, Greece

Abstract

Mobile manipulator systems, comprised of a mobile platform with one or more manipulators, are of great interest in a number of applications. This paper presents a planning and control methodology for such systems allowing them to follow simultaneously desired end-effector and platform trajectories without violating the nonholonomic constraints. Based on a reduction of system dynamics, a model-based controller is designed to eliminate tracking errors without requiring large gains. The sensitivity to parameter errors is examined and found to be negligible. The validity of the methodology is demonstrated using example systems.

1 Introduction

Mobile manipulator systems consist of a mobile platform equipped with manipulators, see Fig. 1. Applications for such systems abound in mining, construction, forestry, planetary exploration and the military.

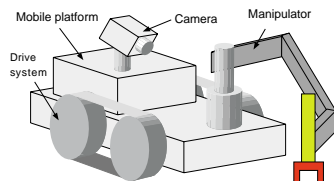


Fig. 1. Mobile manipulator system.

A host of issues related to mobile manipulators have been studied in the past. These include dynamic and static stability, force development and application, control in the presence of base compliance, dynamic coupling issues, etc. see for example [1-4]. However, in these studies, the mobile manipulator system is assumed to be non-moving.

Mobile platforms are subject to nonholonomic constraints that arise from wheel kinematics. Motion planning for mobile platforms is concerned with obtaining open loop controls which steer the platform from an initial state to a final one, without violating the nonholonomic constraints, see for example [5-6]. The emphasis here is in obtaining a desired final state for the driving platform and possibly of its trailers and not in path following. A survey on recent developments in control of nonholonomic systems can be found in [7].

Moving mobile manipulators systems, present many unique problems that are due to the coupling of holonomic manipulators with nonholonomic bases. Seraji presents a simple on-line approach for motion control of mobile manipulators using augmented Jacobian matrices, [8]. The

approach is kinematic and requires additional constraints to be met for the manipulator configuration. The proposed approach can be equally applied to nonholonomic and holonomic mobile robots. Lim and Seraji describe the design and implementation of real-time control system applied on a 7 degree-of-freedom (DOF) arm mounted on a 1-DOF holonomic platform, [9]. The redundant equations are solved using weighted pseudo inverses and a geometry-based control scheme.

The dynamics of nonholonomic systems are more complex compared to those of holonomic ones. Saha and Angeles derived the equations of motion of such systems using a Newton-Euler approach and a natural orthogonal complement of the matrix associated with the velocity constraint equations written in linear homogeneous form, [10]. Sarkar et al. developed a unified approach to the control of mechanical systems subject to holonomic and nonholonomic constraints, [11].

This paper focuses on trajectory planning and control for mobile manipulators. Two commonly available mobile platforms, a car-like and a differentially driven platform, equipped with a two-link manipulator, are used as examples. The system differential kinematics are derived to map platform and end-effector velocities to actuator velocities, without violating the nonholonomic constraints. This allows specifying paths and trajectories for both the platform and the end-effector. Next, orthogonal complements and a Lagrangian approach are used to obtain the reduced equations of motion. A model-based controller is designed for the differentially-driven mobile manipulator that eliminates tracking errors. This controller is relatively insensitive to parameter variations. To illustrate the proposed methodology, an example of crack sealing is studied, in which the end-effector follows a complex path while the platform moves along a smoother path.

2 Kinematic Modeling of Mobile Manipulators

Mobile manipulators can be built based on various mobile platform designs, that differ by the drive mechanism employed. The most commonly available mobile platforms use either a differential drive or a car-like drive. The former employs two independently driven wheels with a common axis, and casters that add stability to the mobile platform. The later is a tricycle design in which the driving front wheel is also used for steering. In this section, we derive the differential kinematic equations for these two types of mobile manipulator systems.

a. Differential-Drive Mobile Manipulator

Consider the mobile manipulator system depicted in Fig. 2.

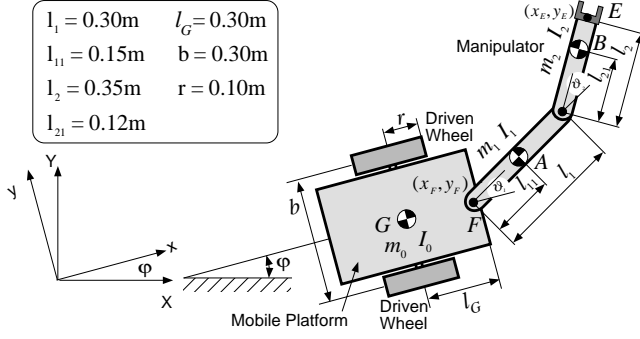


Fig 2. Mobile manipulator system on a differentially-driven platform.

The platform moves by driving the two independent wheels as shown in the figure. On the assumption of low vehicle speeds, the two driven wheels do not slip sideways. The resulting velocity constraint, see [8], for point F, is

$$\dot{x}_F \sin \phi - \dot{y}_F \cos \phi + \dot{\phi} l_G = 0 \quad (1)$$

where l_G is the distance between G and F. It can be shown, see [5], [6], that Eq. (1) is a nonholonomic constraint i.e. a constraint which cannot be integrated analytically.

Focusing on the platform first, the differential kinematics equation relating the wheel rates to the linear velocity of F and to the platform rate of rotation, $\dot{\phi}$, is

$$\begin{bmatrix} \dot{x}_F \\ \dot{y}_F \\ \dot{\phi} \end{bmatrix} = \begin{bmatrix} \frac{r}{2} c\phi + \frac{l_G \cdot r}{b} s\phi & \frac{r}{2} c\phi - \frac{l_G \cdot r}{b} s\phi \\ \frac{r}{2} s\phi - \frac{l_G \cdot r}{b} c\phi & \frac{r}{2} s\phi + \frac{l_G \cdot r}{b} c\phi \\ -\frac{r}{b} & \frac{r}{b} \end{bmatrix} \begin{bmatrix} \dot{\vartheta}_\ell \\ \dot{\vartheta}_r \end{bmatrix} \quad (2)$$

where $\dot{\vartheta}_\ell$ and $\dot{\vartheta}_r$ are the angular velocities of the left and right wheels respectively and the symbols c and s have been used instead of cos and sin. The two angular velocities are mapped to the three system velocities. Furthermore, in contrast to car-like mobile platforms, this type of platform has the ability to change its orientation on the spot.

Keeping the first two equations in matrix Eq. (2) and displaying the rotation matrix explicitly, we can write

$$\begin{bmatrix} \dot{x}_F \\ \dot{y}_F \end{bmatrix} = \begin{bmatrix} c\phi & -s\phi \\ s\phi & c\phi \end{bmatrix} \begin{bmatrix} \frac{r}{2} & \frac{r}{2} \\ -\frac{l_G \cdot r}{b} & \frac{l_G \cdot r}{b} \end{bmatrix} \begin{bmatrix} \dot{\vartheta}_\ell \\ \dot{\vartheta}_r \end{bmatrix} \quad (3)$$

From this equation we observe that if $l_G = 0$, i.e. if the manipulator is mounted on the axis that connects the wheel centers, then the second matrix in Eq. (3) becomes singular. This is because all points along this axis must have a velocity perpendicular to it, and therefore, one degree of freedom is lost. Mounting the manipulator away from this axis removes this problem.

The linear velocity of the end effector is found using the fact that its base velocity is known and given by Eq.

(3). Therefore, the end-effector velocity is written as

$$\begin{bmatrix} \dot{x}_E \\ \dot{y}_E \end{bmatrix} = \begin{bmatrix} \dot{x}_F \\ \dot{y}_F \end{bmatrix} + \begin{bmatrix} c\phi & -s\phi \\ s\phi & c\phi \end{bmatrix} \begin{bmatrix} J_{11} & J_{12} \\ J_{21} & J_{22} \end{bmatrix} \begin{bmatrix} \dot{\vartheta}_1 + \dot{\phi} \\ \dot{\vartheta}_2 \end{bmatrix} \quad (4)$$

where \dot{x}_E, \dot{y}_E are the x and y components of the velocity of E, and the J_{ij} (i, j = 1,2) terms are the elements of the fixed-base Jacobian of the manipulator employed, given by

$$J_{11} = -l_1 \sin(\vartheta_1) - l_2 \sin(\vartheta_1 + \vartheta_2) \quad (5a)$$

$$J_{12} = -l_2 \sin(\vartheta_1 + \vartheta_2) \quad (5b)$$

$$J_{21} = l_1 \cos(\vartheta_1) + l_2 \cos(\vartheta_1 + \vartheta_2) \quad (5c)$$

$$J_{22} = l_2 \cos(\vartheta_1 + \vartheta_2) \quad (5d)$$

where l_1, l_2 , are the lengths of the upper arm, and the forearm respectively, and ϑ_1, ϑ_2 , are the joint variables of the manipulator, see Fig. 2.

Note that the platform rotation rate, $\dot{\phi}$, is still present in Eq. (4), as an input term. By writing the platform rotation rate in terms of the wheel rates, using the third equation from Eq. (2), and combining Eqs. (3) and (4), the forward differential kinematics of the system is obtained as

$$\begin{bmatrix} \dot{x}_E \\ \dot{y}_E \\ \dot{x}_F \\ \dot{y}_F \end{bmatrix} = \begin{bmatrix} c\phi & -s\phi & 0 & 0 \\ s\phi & c\phi & 0 & 0 \\ 0 & 0 & c\phi & -s\phi \\ 0 & 0 & s\phi & c\phi \end{bmatrix} \begin{bmatrix} \dot{\vartheta}_\ell \\ \dot{\vartheta}_r \\ \dot{\vartheta}_1 \\ \dot{\vartheta}_2 \end{bmatrix} \quad (6a)$$

$$\begin{bmatrix} r/2 - J_{11}r/b & r/2 + J_{11}r/b & J_{11} & J_{12} \\ -(l_G + J_{21})r/b & (l_G + J_{21})r/b & J_{21} & J_{22} \\ r/2 & r/2 & 0 & 0 \\ -l_G r/b & l_G r/b & 0 & 0 \end{bmatrix} \begin{bmatrix} \dot{\vartheta}_\ell \\ \dot{\vartheta}_r \\ \dot{\vartheta}_1 \\ \dot{\vartheta}_2 \end{bmatrix} \Rightarrow \dot{\mathbf{x}} = \mathbf{R} \mathbf{J}_a \dot{\mathbf{v}} = \mathbf{J}_1 \dot{\mathbf{v}} \quad (6b)$$

b. Car-like Mobile Manipulator

Next, consider a simple mobile manipulator system whose platform includes a front and two rear wheels, see Fig. 3. The rear wheels are parallel to the main axis of the car while the front wheel is used for steering the platform. Again, the wheels do not slip sideways.

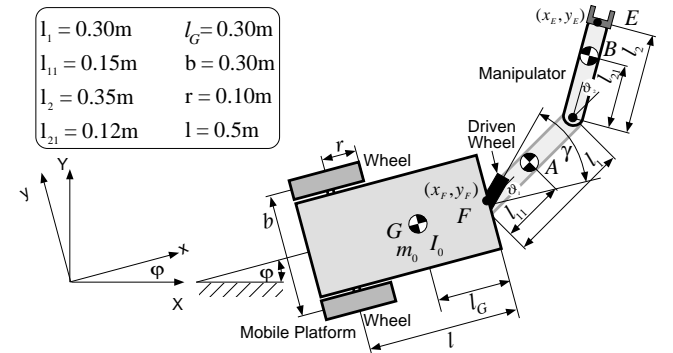


Fig. 3. Car-like mobile manipulator system.

For simplicity, the manipulator is mounted at point F, where the steering wheel is located also. For this point the

nonholonomic constraint is written as

$$\dot{x}_F \sin \varphi - \dot{y}_F \cos \varphi + \dot{\varphi} l = 0 \quad (7)$$

where \dot{x}_F and \dot{y}_F are the x and y components of the velocity v_F of point F respectively, and l is the distance between the point F and the back wheel axis.

The differential kinematics of the car-like mobile platform are described by the following matrix equation

$$\begin{bmatrix} \dot{x}_F \\ \dot{y}_F \\ \dot{\varphi} \end{bmatrix} = \begin{bmatrix} \cos(\varphi + \gamma) & 0 \\ \sin(\varphi + \gamma) & 0 \\ l^{-1} \cdot \sin \gamma & 0 \end{bmatrix} \begin{bmatrix} v_F \\ \dot{\gamma} \end{bmatrix} \quad (8)$$

where γ is the steering angle, $v_F = \omega r$ is the velocity due to the driving wheel at F, ω is the front wheel angular rate, and r is its radius. The zero column of the matrix in Eq. (8) shows that if the mobile platform is not moving ($v_F = 0$) then neither the position nor the orientation of the platform can be changed using the steering wheel.

Eq. (8) is in a form not suitable for planning because its Jacobian contains a zero column. To solve this problem, the first two equations in Eq. (8) are rewritten as follows

$$\begin{bmatrix} \dot{x}_F \\ \dot{y}_F \end{bmatrix} = \begin{bmatrix} c\varphi & -s\varphi \\ s\varphi & c\varphi \end{bmatrix} \begin{bmatrix} r & 0 \\ 0 & r \end{bmatrix} \begin{bmatrix} \omega \cos \gamma \\ \omega \sin \gamma \end{bmatrix} \quad (9)$$

Note that this change of input velocities gives a Jacobian form that is always invertible. As for the differentially-driven system, the end-effector velocity is given by

$$\begin{bmatrix} \dot{x}_E \\ \dot{y}_E \end{bmatrix} = \begin{bmatrix} \dot{x}_F \\ \dot{y}_F \end{bmatrix} + \begin{bmatrix} c\varphi & -s\varphi \\ s\varphi & c\varphi \end{bmatrix} \begin{bmatrix} J_{11} & J_{12} \\ J_{21} & J_{22} \end{bmatrix} \begin{bmatrix} \dot{\vartheta}_1 + \dot{\varphi} \\ \dot{\vartheta}_2 \end{bmatrix} \quad (10)$$

where the J_{ij} , ($i, j = 1, 2$) are defined in Eqs. (5).

Next, the platform rotation rate $\dot{\varphi}$ is substituted using the third line of the matrix Eq. (8) while the resulting equation is appended to Eq. (9) to yield the system differential kinematics

$$\begin{bmatrix} \dot{x}_E \\ \dot{y}_E \\ \dot{x}_F \\ \dot{y}_F \end{bmatrix} = \begin{bmatrix} c\varphi & -s\varphi & 0 & 0 \\ s\varphi & c\varphi & 0 & 0 \\ 0 & 0 & c\varphi & -s\varphi \\ 0 & 0 & s\varphi & c\varphi \end{bmatrix} \begin{bmatrix} J_{11} & J_{12} & r & \frac{r}{l} J_{11} \\ J_{21} & J_{22} & 0 & r + \frac{r}{l} J_{21} \\ 0 & 0 & r & 0 \\ 0 & 0 & 0 & r \end{bmatrix} \begin{bmatrix} \dot{\vartheta}_1 \\ \dot{\vartheta}_2 \\ \omega \cdot c\gamma \\ \omega \cdot s\gamma \end{bmatrix} \quad (11a)$$

$$\Rightarrow \dot{\mathbf{x}} = \mathbf{R} \mathbf{J}_b \Omega = \mathbf{J}_2 \Omega \quad (11b)$$

where Ω corresponds to the last column vector in Eq. (11a) and the remaining variables have been defined before.

3 End-effector - Platform Path Planning

The task we tackle in this section is to generate the desired driven wheel rate inputs so that the platform and the end-effector follow given trajectories. A typical application for this problem is the robotic crack-sealing, where a robotic mobile platform is required to follow a given path, while the end-effector must follow some crack on the pavement.

Eqs. (6) and (11) can be used to generate desired input velocities so that the platform and the manipulator's end-effector both follow desired trajectories. Since both

equations take into account the nonholonomic constraints, the computed wheel speeds result in motions that do not violate the nonholonomic constraint and therefore are achievable by the mobile manipulator system. The platform angular velocity $\dot{\varphi}$ is found using the last equation in Eq. (2) or Eq. (8). The platform orientation is found by integrating this angular velocity. We assume that the shape of the crack to follow is available. Setting some time in which the task must be accomplished results in the desired end-effector trajectory described by $x_{E,d}(t)$ and $y_{E,d}(x_{E,d})$.

The curve followed by the point F on the platform either is arbitrarily specified on the condition that the distance between (x_E, y_E) and (x_F, y_F) is within the reach of the manipulator, or corresponds to a prescribed path for which the same condition follows. Otherwise, the task is not feasible and a singularity will occur. Indeed, the Jacobians \mathbf{J}_a and \mathbf{J}_b become singular when

$$\det \mathbf{J}_a = \frac{l_G l_1 l_2 r^2 \sin \vartheta_2}{b} = 0 \Rightarrow \vartheta_2 = 0^\circ, \pm 180^\circ \quad (12)$$

$$\det \mathbf{J}_b = l_1 l_2 r^2 \sin \vartheta_2 = 0 \Rightarrow \vartheta_2 = 0^\circ, \pm 180^\circ \quad (13)$$

which means that a singularity arises when the manipulator is fully extended or folded. Indeed, in such case the desired location for E is not within the reach of the manipulator, and a tool at E cannot follow the desired path (crack). This problem can be overcome by re-planning the path of F. Moreover, it is advantageous to choose the motion of point F so that it is smooth and that its curvature does not violate any steering angle constraints.

Although the inversion of the kinematic equations results in desired wheel rates, one has to control such a mobile manipulator system by applying the proper torques that will eliminate any trajectory errors. The control design should take into account the mass properties of the mobile system. Therefore, in the next section we derive the equations of motion for the differentially-driven system.

4 Dynamics of the Differential-Drive Mobile Manipulator System

Applying Lagrange's equations of motion directly cannot yield the dynamics of mechanical systems subject to nonholonomic constraints. Additional terms describing the constraint forces must be added, see [10], [11].

The system under consideration is subject to a single nonholonomic constraint, which is described by Eq. (1). This equation can be written in matrix form as

$$\mathbf{A}(\mathbf{q})\dot{\mathbf{q}} = 0 \quad (14)$$

where,

$$\mathbf{A}(\mathbf{q}) = \begin{bmatrix} \sin \varphi & -\cos \varphi & l_G & 0 & 0 \end{bmatrix}$$

$$\dot{\mathbf{q}} = \begin{bmatrix} \dot{x}_F & \dot{y}_F & \dot{\varphi} & \dot{\vartheta}_1 & \dot{\vartheta}_2 \end{bmatrix}^T$$

To derive the equations of motion for the mobile manipulator system, first let $L(\mathbf{q}, \dot{\mathbf{q}})$ represent the unconstrained system Lagrangian. Assuming that the mass and the moments of inertia of the casters and the driving wheels are negligible, this is equal to

$$L = \frac{1}{2}m_0(\dot{x}_G^2 + \dot{y}_G^2) + \frac{1}{2}J_0\dot{\varphi}^2 + \frac{1}{2}m_1(\dot{x}_A^2 + \dot{y}_A^2) + \frac{1}{2}J_1(\dot{\varphi} + \dot{\vartheta}_1)^2 + \frac{1}{2}m_2(\dot{x}_B^2 + \dot{y}_B^2) + \frac{1}{2}J_2(\dot{\varphi} + \dot{\vartheta}_1 + \dot{\vartheta}_2)^2 \quad (15)$$

where $m_0, m_1, m_2, J_0, J_1, J_2$ are the masses and the moments of inertia of the platform, the first and the second link respectively, and $\dot{x}_G, \dot{y}_G, \dot{x}_A, \dot{y}_A, \dot{x}_B, \dot{y}_B$, the x , and y components of the velocities of the center of mass of the platform, and the first and the second link respectively.

Adding constraint forces as input terms forms the equations of motion of the constrained system. Here, these forces are responsible for not allowing the wheels to slip sideways. The constrained dynamics are written as

$$\frac{d}{dt} \frac{\partial L}{\partial \dot{\mathbf{q}}} - \frac{\partial L}{\partial \mathbf{q}} + \mathbf{A}^T(\mathbf{q})\lambda - \boldsymbol{\xi} = \mathbf{0} \quad (16)$$

where $\mathbf{q} = [x_F \ y_F \ \varphi \ \vartheta_1 \ \vartheta_2]^T$ are the generalized coordinates, λ is the Lagrange multiplier that corresponds to the constraint force, and $\boldsymbol{\xi}$ represents the externally applied forces. The columns of \mathbf{A}^T form a non-normalized base for these forces.

Expressing Eq. (15) in terms of the generalized coordinates and substituting the result into Eq. (16), the system equations of motion are obtained in the form

$$\mathbf{M}(\mathbf{q})\ddot{\mathbf{q}} + \mathbf{V}(\mathbf{q}, \dot{\mathbf{q}}) = \mathbf{E}(\mathbf{q})\boldsymbol{\tau} - \mathbf{A}^T(\mathbf{q})\lambda \quad (17)$$

where $\mathbf{M}(\mathbf{q})$ is the 5x5 inertia matrix, $\mathbf{V}(\mathbf{q}, \dot{\mathbf{q}})$ is the vector of velocity-dependent forces, $\boldsymbol{\tau} = [\tau_i, \tau_r, \tau_1, \tau_2]^T$ is the 4-dimensional torque vector, $\mathbf{E}(\mathbf{q})$ is a 5x4 input transformation matrix, comprised of the left and right wheel torques and the first and second manipulator joint torques, and λ is the Lagrange multiplier.

Eq. (14) shows that the constraint velocity is always in the nullspace of $\mathbf{A}(\mathbf{q})$, so it is possible to define 5-1=4 independent velocities $\dot{\mathbf{v}}(t) = [\dot{v}_1, \dot{v}_2, \dot{v}_3, \dot{v}_4]^T$ such that

$$\dot{\mathbf{q}} = \mathbf{S}(\mathbf{q})\dot{\mathbf{v}}(t) \quad (18)$$

where the matrix $\mathbf{S}(\mathbf{q})$ contains the base vectors of the nullspace of \mathbf{A} . The selection of the base of the nullspace is important and allows the independent velocities to have a physical meaning. For our system, we choose $\mathbf{S}(\mathbf{q})$ to be

$$\mathbf{S} = \begin{bmatrix} \frac{r \cdot c \varphi}{2} + \frac{l_G r \cdot s \varphi}{b} & \frac{r \cdot c \varphi}{2} - \frac{l_G r \cdot s \varphi}{b} & 0 & 0 \\ \frac{r \cdot s \varphi}{2} - \frac{l_G r \cdot c \varphi}{b} & \frac{r \cdot s \varphi}{2} + \frac{l_G r \cdot c \varphi}{b} & 0 & 0 \\ -r/b & r/b & 0 & 0 \\ 0 & 0 & 1 & 0 \\ 0 & 0 & 0 & 1 \end{bmatrix} \quad (19)$$

of rank 4 since $\det(\mathbf{S}^T \mathbf{S}) = (1 + l_G^2)r^2/b^2 \neq 0$. The vector of the independent velocities is

$$\dot{\mathbf{v}} = [\dot{v}_i \ \dot{v}_r \ \dot{v}_1 \ \dot{v}_2]^T$$

Differentiating Eq. (18), substituting the expression for $\ddot{\mathbf{q}}$ into Eq. (17) and premultiplying by \mathbf{S}^T , yields

$$\mathbf{S}^T(\mathbf{M}\ddot{\mathbf{v}}(t) + \mathbf{M}\dot{\mathbf{S}}\dot{\mathbf{v}}(t) + \mathbf{V}) = \mathbf{S}^T \mathbf{E} \boldsymbol{\tau} \quad (20)$$

Note that since $\mathbf{S} \in N(\mathbf{A})$, $\mathbf{S}^T \mathbf{A}^T \lambda$ vanishes from the above equation. Equation (20) is further written as

$$\mathbf{M}^* \ddot{\mathbf{v}} + \mathbf{V}^* = \mathbf{E}^* \boldsymbol{\tau} \quad (21)$$

where $\mathbf{M}^* = \mathbf{S}^T \mathbf{M} \mathbf{S}$, $\mathbf{V}^* = \mathbf{S}^T(\mathbf{M}\dot{\mathbf{S}}\dot{\mathbf{v}} + \mathbf{V})$, and $\mathbf{E}^* = \mathbf{S}^T \mathbf{E} = \mathbf{I}_{4 \times 4}$, i.e. the identity 4x4 matrix. Since \mathbf{S} is non-singular, the reduced mass matrix \mathbf{M}^* is always symmetric and positive definite.

Eq. (21) can be transformed further in the operational space using Eq. (6). The result is

$$\bar{\mathbf{M}}\ddot{\mathbf{x}} + \bar{\mathbf{V}} = \mathbf{F} = \mathbf{J}_1^{-T} \boldsymbol{\tau} \quad (22)$$

where $\bar{\mathbf{M}} = \mathbf{J}_1^{-T} \mathbf{M}^* \mathbf{J}_1^{-1}$ and $\bar{\mathbf{V}}$ contains all the velocity terms. Eq. (22) is in a very useful form because it links the four input torques to the four output accelerations.

5 Model-based Control Design

Eq. (22) is in the form of holonomic mechanical systems and can be easily used for model based control of the system. To this end, we use the following control scheme

$$\boldsymbol{\tau} = \mathbf{J}_1^T(\bar{\mathbf{M}}\ddot{\mathbf{x}}^* + \bar{\mathbf{V}}) \quad (23)$$

where the auxiliary accelerations are given by

$$\ddot{\mathbf{x}}^* = \ddot{\mathbf{x}}_d + \mathbf{K}_v(\dot{\mathbf{x}}_d - \dot{\mathbf{x}}) + \mathbf{K}_p(\mathbf{x}_d - \mathbf{x}) \quad (24)$$

In Eq. (24), the subscript d corresponds to desired values, and \mathbf{K}_v and \mathbf{K}_p are diagonal gain matrices

$$\mathbf{K}_v = \text{diag}\{k_{vi}\}, \quad \mathbf{K}_p = \text{diag}\{k_{pi}\}$$

Assuming exact parameter knowledge, substituting Eq. (24) into Eq. (23), and applying the resulting torques to the system equations of motion, the error dynamics are

$$\ddot{e}_i + k_{vi}\dot{e}_i + k_{pi}e_i = 0, \quad i = 1, \dots, 4 \quad (25)$$

where $e_i = x_{i,d} - x_i$. These equations, which are linear and decoupled, permit the selection of the elements of the gain matrices \mathbf{K}_v and \mathbf{K}_p so as to have the error eliminated according to given specifications.

In the case of parameter errors, the control vector is

$$\boldsymbol{\tau} = \hat{\mathbf{J}}_1^T(\hat{\bar{\mathbf{M}}}\ddot{\mathbf{x}}^* + \hat{\bar{\mathbf{V}}}) \quad (26)$$

where $\hat{\bar{\mathbf{M}}}$ and $\hat{\bar{\mathbf{V}}}$ represent the estimates of the terms in the dynamical model. Using Eq. (26) as a nonlinear control law and taking the new input vector to be as in Eq. (24), we get

$$\ddot{\mathbf{e}} + \mathbf{K}_d \dot{\mathbf{e}} + \mathbf{K}_p \mathbf{e} = \mathbf{d} \quad (27)$$

where

$$\mathbf{d} = \left(\mathbf{I} - (\hat{\mathbf{J}}_1^T \hat{\bar{\mathbf{M}}})^{-1} (\hat{\mathbf{J}}_1^T \hat{\bar{\mathbf{M}}}) \right) \ddot{\mathbf{x}}^* - (\hat{\mathbf{J}}_1^T \hat{\bar{\mathbf{M}}})^{-1} (\hat{\mathbf{J}}_1^T \hat{\bar{\mathbf{V}}} - \bar{\mathbf{V}}) \quad (28)$$

The system described by Eq. (27) is nonlinear and coupled while the error convergence is not ensured due to the term on the right hand side.

6 Simulation Results

a. Trajectory Planning

First, the trajectories for the two mobile manipulators shown in Figs. 2 and 3 are planned. Their kinematics parameters are displayed in the same figures. For trajectory planning, the desired motion time was chosen equal to 6s (so as to yield reasonable velocities) and the initial posture of the system was $(x_E^{in}, y_E^{in}, \phi^{in}, \vartheta_1^{in}, \vartheta_2^{in}) = (0.5\text{m}, 0.5\text{m}, 120^\circ, -30^\circ, -20^\circ)$. The final positions for points F and E were $(x_E^{fin}, y_E^{fin}, x_F^{fin}, y_F^{fin}) = (2\text{m}, -2\text{m}, 1.9\text{m}, -1.9\text{m})$. The path for point F on the mobile platform was constructed using a third order polynomial for the time parameterization of x_F and a second order polynomial for $y_F=f(x_F)$. The given path for the end-effector and the platform are shown in Fig. 4. Figs. 5 and 6 present snapshots of the motion of the differentially-driven and the car-like mobile system respectively. In general both systems react in the same way.

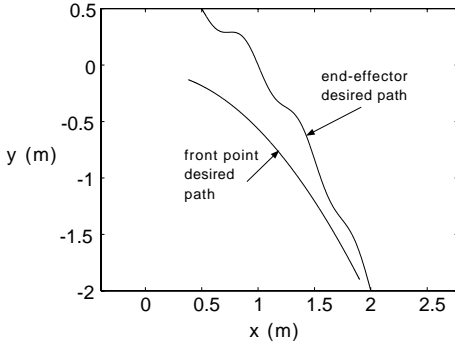


Fig. 4. Desired platform and end-effector paths.

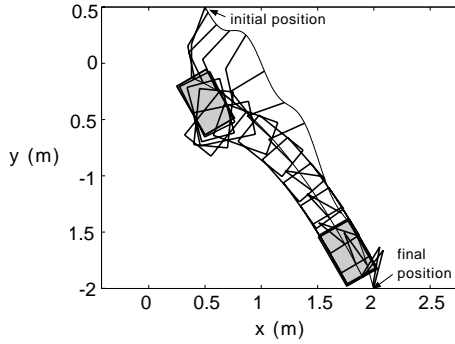


Fig. 5. Animation of the motion of the mobile manipulator with a differential drive.

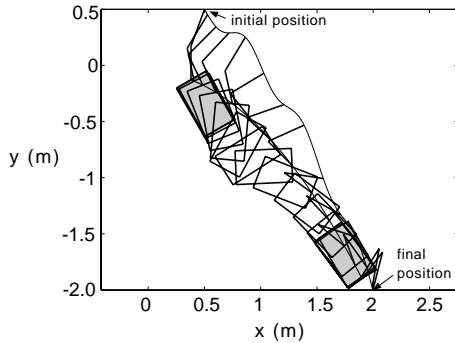


Fig. 6. Animation of the motion of the mobile manipulator with car-like drive.

However the cusp that appears in those figures takes place in different positions and has a different shape. It can be seen that the cusp of the differentially-driven mobile manipulator is sharper than that of the car-like one. This is not surprising as the differentially-driven system has the ability to turn on the spot.

b. Dynamics and Model-based Control

Next, we apply the model-based control algorithm to the differentially driven mobile manipulator using the desired trajectories in Section 6a. The system mass properties are displayed in Table I.

Table I. Mobile manipulator mass properties

Parameter	Value	Units
m_0	50.0	kg
m_1	4.0	kg
m_2	3.5	kg
J_0	1.417	kg m ²
J_1	0.030	kg m ²
J_2	0.036	kg m ²

The controller gains are selected to force the error dynamics exhibit a critical response with a settling time equal to 1 s. The resulting gain matrices are

$$\mathbf{K}_v = \text{diag}\{12\} \text{ and } \mathbf{K}_p = \text{diag}\{36\}$$

Fig. 7 shows the torques applied on the two driven wheels while Fig. 8 shows the torques applied on the joints of the manipulator. As expected, small initial end-effector and platform errors were eliminated by the controller, without requiring excessive control gains.

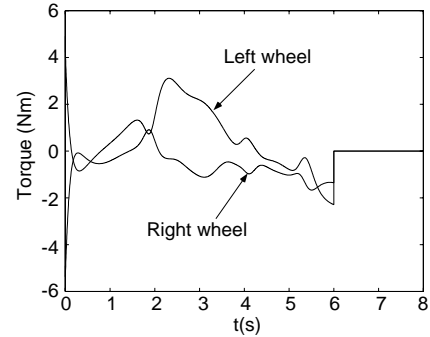


Fig. 7. Driving wheel torques.

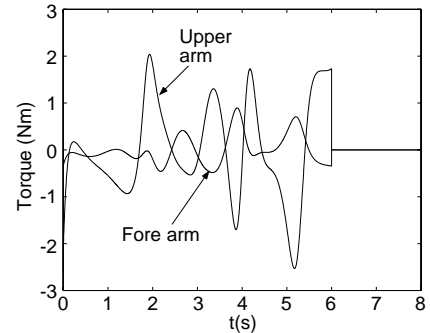


Fig. 8. Manipulator torques.

If the exact values of the kinematics and dynamics parameters are not known, the proposed controller is still valid, on the condition of small uncertainties. This is illustrated in Figs. 9-11, where parameter uncertainties of the order of 3-5% were introduced. In Fig. 9, the history of the position errors for the end-effector and for the front point F of the platform are shown for an 8s runtime and for the same initial error as before. It can be seen that the tracking errors converge to zero, although their responses deviate from the ones where system parameters are known. Figs. 9 and 10 depict the resulting joint and wheel torques, compare with Figs. 7 & 8.

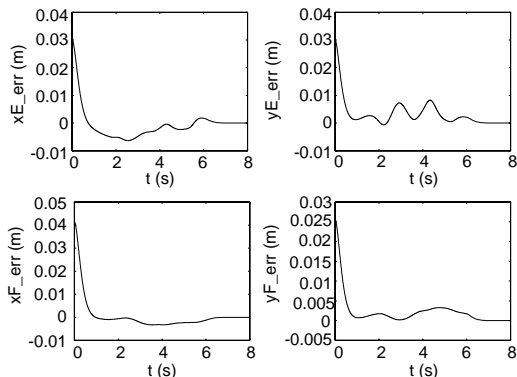


Fig. 9. Errors with parameter uncertainties.

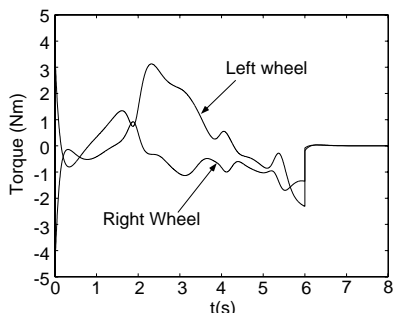


Fig. 10. Driving wheel torques with uncertainties.

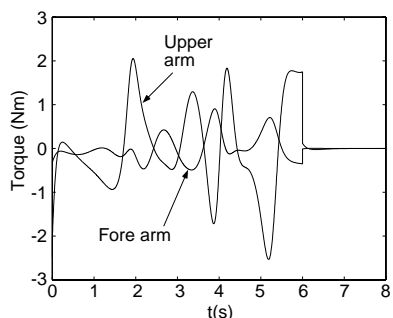


Fig. 11. Manipulator torques with uncertainties.

7 Conclusions

This paper focused on trajectory following and control of mobile manipulators, using as examples a car-like and a differentially-driven system. Both system platforms were equipped with a two link manipulator. The differential

kinematics for the two mobile systems were written so as to map platform and end-effector velocities to driven wheel velocities, without violation of the nonholonomic constraints. This allowed specification of trajectories for both the platform and the end-effector and computation of actuator commands. Orthogonal complements and the Lagrangian methodology were used to obtain the reduced equations of motion for the differentially-driven system. Based on these equations, a model-based controller was designed to eliminate tracking errors. The controller was applied successfully to a simple crack-sealing example. Finally, the controller was shown to be relatively insensitive to small parameter variations.

References

- [1] Papadopoulos, E. and Rey, D., "A New Measure of Tipover Stability Margin for Mobile Manipulators," *Proc. IEEE Int. Conf. on Robotics and Automation*, Minneapolis, MN, April 1996, pp. 3111-3116.
- [2] Papadopoulos, E. and Gonthier, Y., "A Framework for Large-Force Task Planning of Mobile Redundant Manipulators," *J. of Robotic Systems*, Vol. 16, No. 3, 1999, pp. 151-162.
- [3] Hootsmans, N. A. and Dubowsky, S., "Large Motion Control of Mobile Manipulators Including Vehicle Suspension Characteristics," *Proc. Int. Conference on Robotics and Automation*, Sacramento, CA, April 1991, pp. 2336-2341.
- [4] Wiens, G., J., "Effects of Dynamic Coupling in Mobile Robotic Systems," *Proc. ASME Robotics Research World Conference*, Gaithersburg, MI, May 1989, pp. 3-43:3-57.
- [5] Lafferiere G. and Sussmann H., "Motion Planning for Controllable Systems without Drift," *Proc. IEEE Int. Conference on Robotics and Automation*, April 1991, Sacramento, CA, pp. 1148-1153.
- [6] Murray R. and Sastry S. S., "Nonholonomic Motion Panning: Steering using Sinusoids," *Trans. on Robotics and Automation*, Vol. 38, No. 5, May 1993, pp.700-716.
- [7] Kolmanovsky I. and McClamroch, H., "Developments in Nonholonomic Control Problems," *IEEE Control Systems*, December 1995, pp. 20-35.
- [8] Seraji H., "A Unified Approach to Motion Control of Mobile Manipulators," *Int. J. Robotics Research*, Vol. 17, No. 2, February 1998, pp. 107-118.
- [9] Lim D. and Seraji H., "Configuration Control of a Mobile Dexterous Robot: Real-Time Implementation and Experimentation," *Int. J. Robotics Research*, Vol. 16, No. 5, October 1997, pp. 601-618.
- [10] Saha K. S. and Angeles J., "Dynamics of Nonholonomic Mechanical Systems using a Natural Orthogonal Complement," *ASME J. of Applied Mechanics*, March 1991, Vol. 58, pp. 238-243.
- [11] Sarkar N, Yun X. and Kumar V., "Control of Mechanical Systems with Rolling Constraints: Application to Dynamic Control of Mobile Robots," *Int. J. Robotics Research*, Vol. 13, No. 1, February 1994, pp. 55-69.